Probing the kinetic and thermodynamic consequences of the tetraloop/tetraloop receptor monovalent ion-binding site in P4–P6 RNA by smFRET

Namita Bisaria* and Daniel Herschlag*[1]

*Department of Biochemistry, Stanford University, Stanford, CA 94305, U.S.A.

Abstract

Structured RNA molecules play roles in central biological processes and understanding the basic forces and features that govern RNA folding kinetics and thermodynamics can help elucidate principles that underlie biological function. Here we investigate one such feature, the specific interaction of monovalent cations with a structured RNA, the P4–P6 domain of the *Tetrahymena* ribozyme. We employ single molecule FRET (smFRET) approaches as these allow determination of folding equilibrium and rate constants over a wide range of stabilities and thus allow direct comparisons without the need for extrapolation. These experiments provide additional evidence for specific binding of monovalent cations, Na^+ and K^+, to the RNA tetraloop–tetraloop receptor (TL–TLR) tertiary motif. These ions facilitate both folding and unfolding, consistent with an ability to help order the TLR for binding and further stabilize the tertiary contact subsequent to attainment of the folding transition state.

Introduction

RNA molecules play roles beyond acting as simple intermediaries in information flow from DNA to proteins and numerous RNAs adopt folded structures in order to function [1]. These RNAs, in conjunction with associated proteins, function in epigenetics and genome maintenance [2,3], pre-mRNA splicing [4], RNA processing [5], gene expression regulation [6], protein synthesis [7], and protein transport [8]. It is important to study these complex macromolecular machines directly and also to uncover the physical features and forces that mediate their folding through systematic and controlled investigation of simpler, model RNA systems (e.g., [9–11]).

All RNAs, as polyelectrolytes, are subject to electrostatic interactions that disfavour folding and typically favour RNA–protein interactions [12,13]. Thus, these processes cannot be understood without deciphering electrostatics. Electrostatic interaction energies are modulated by a surrounding ion atmosphere and higher concentrations of ions and higher ion valences generally better screen charge and enhance RNA folding [11,13–17]. Ions can also directly bind to RNA molecules, and several metal ion binding sites on RNA have been identified through structural and functional studies (e.g., [18–25]). Distinguishing effects of ions in the atmosphere from those that are site bound is a major but

necessary challenge in dissecting electrostatic interactions and effects (e.g., [21,24,26–29]).

Most attention on specific metal-ion binding has focused on divalent metal ions and, in particular, Mg^{2+}, as it represents the predominant cellular divalent metal ion. In principle, if monovalent ions only occupied the ion atmosphere and did not engage in specific interactions with RNA, they could be used simply to modulate charge screening through the ion atmosphere. However, there is compelling evidence for greater complexity of monovalent cation effects in RNA folding [30].

Monovalent cations preferentially occupy the ion atmosphere of a simple DNA helix inversely as a function of size [11] and studies on the relaxation of short DNA helices attached by a short, flexible, linker revealed the same trend [31]. However, Draper and colleagues [30] observed monovalent ion preferences for the folding of several RNAs that were distinct from size order obtained in the helix systems and different from one another. One of the RNAs exhibiting such a distinct behaviour, so-called 'tecto-RNA' [32], involves the association of two RNA pieces via two tetraloop–tetraloop receptor (TL–TLR) tertiary motifs. TL–TLR tertiary motifs are found in many structured RNAs [33] and prior studies with the P4–P6 RNA had provided evidence for a specific K^+-binding site within its TL–TLR (Figure 1C; [18,34]).

P4–P6 is an independently folding RNA derived from the *Tetrahymena* group I intron, with two sets of coaxially stacked helices, a sharp bend mediated by the J5/5a junction and two tertiary interactions that connect the helical stacks, a

Figure 1 | P4–P6 RNA and its crystallographic K$^+$ ion-binding site

(**A**) Secondary structure of the P4–P6 domain. Tertiary contacts are coloured, the TL–TLR (green) and the MC–MCR (blue). Dye placements for smFRET are shown, Cy3 (light green) and Cy5 (maroon). A mutation used to disrupt the monovalent ion-binding site, A225U, is highlighted in red. Fluorescently-labelled P4–P6 molecules used in smFRET experiments were generated using splinted ligation of synthetic and transcribed RNA pieces, as described in [48,49]. (**B**) P4–P6 tertiary structure rendering based on the PDB: 1GID [35]. Tertiary contacts coloured as in (**A**). (**C**) Monovalent ion-binding site in the TLR of the *Azoarcus* group I intron, rendering from structure (PDB: 1T42, [42]). The same residues are found in the TLR in P4–P6 RNA and numbering from P4–P6 is used in the figure. The mutated residue, A225U, is coloured in red.
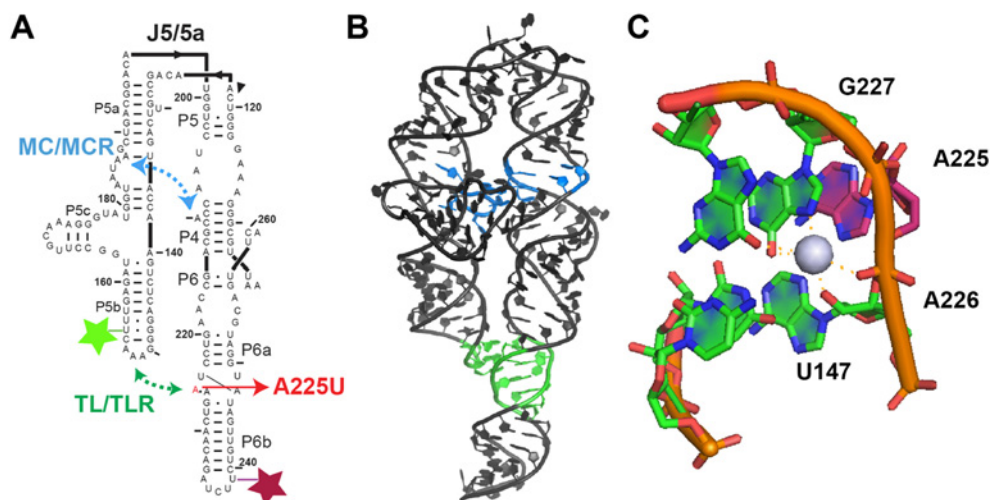
Equilibrium effects of monovalent ions on P4–P6 folding

Figure 2(A) shows the equilibrium folding of P4–P6 RNA in a series of monovalent salts each present at 1.8 M for wild-type P4–P6 and A225U mutant P4–P6 (Figure 1A). P4–P6 RNA folds in ~1 mM Mg^{2+}, but requires higher concentrations of monovalent cation to fold, because monovalent cations are much less effective in charge screening of polyelectrolytes than higher valency cations and because the stabilizing MC–MCR tertiary interaction only forms in the presence of some divalent cations [14,19,26]. For each RNA, under each condition we show the cumulative FRET distribution for all of the molecules, with individual and combined fits to a two-Gaussian model (Figure 2A). The folding and unfolding rate constants are shown in Figure 2(B) for each condition, with the values obtained for each molecule plotted and demonstrating good agreement across the molecular populations studied. Indeed, one of the reasons we chose P4–P6 for in-depth and focused biophysical studies is the

ability to obtain pure and homogeneous populations of this RNA [39].

As expected for a model that describes the data well, there is good agreement between the equilibrium constants obtained from the ratio of rate constants and those obtained directly from the fraction of time spent in high and low FRET states (Table 1). smFRET exhibits an extended dynamic range relative to bulk measurements [40] and we could obtain high precision measurements over equilibrium constants ranging from 0.03 to 20, nearly three orders of magnitude. Nevertheless, we were unable to reliably detect any folded mutant P4–P6 in Cs$^+$ and thus can only report a limit for this equilibrium constant based on a fit to the overall FRET distribution and we could not determine values for its folding and unfolding rate constants.

The folding equilibrium for P4–P6 is plotted as a function of hydrated cation radius in Figure 3(A). As expected based on simple ion size considerations, the order of folding stability for wild-type P4–P6 is as follows: Na$^+$ ~K$^+$ > Rb$^+$ > Cs$^+$. However, Li$^+$ would be expected to give greater folding stability than Na$^+$ or K$^+$, but instead gives an ~7-fold less favourable folding equilibrium (Figure 3A, black; Table 1). This deviation suggests that at least one cation engages in specific and stabilizing interactions with unfolded or folded P4–P6. To further probe the origin of this deviation, we investigated the folding of the A225U mutant of P4–P6. There was prior evidence that mutations in the TLR disrupts the monovalent cation-binding site (Figures 1A and 1C; [18,30]). A225U forms an 'A-platform' [41] with A226 that sits directly below the monovalent cation-binding site; this

Figure 2 | P4–P6 folding thermodynamics and kinetics in different monovalent ion solutions

(**A**) Distribution of FRET intensity for all traces at each condition (grey). FRET intensity is defined as the intensity of each molecule in the acceptor channel divided by the intensity found in both the donor and the acceptor channels. The apparent FRET values range from < 0 to > 1 as a result of varying background and noise contributions. The FRET intensity distribution was fit with a two-Gaussian model (overlay in black), representing the fraction of total time the population of molecules spend in the high FRET state (red line) compared with the low FRET state (green line). (**B**) Scatter plots of the folding compared with unfolding rate constants for each molecule selected under each condition. The mean values for each rate constant are shown in red. Rate constants were determined by analysing each FRET trace with the SMART (Single Molecule Analysis Research Tool) analysis data package, which utilizes a hidden Markov modelling-based algorithm that fits single-molecule trace data to kinetic models [47]. For P4–P6 folding, a simple two-state model was used. smFRET imaging, trace selection and processing was done as described previously [49,50], using a custom total internal reflection (TIRF) setup with image acquisition by Andor iXon Ultra camera and the Nikon Elements software. All smFRET data were taken with a 20 ms exposure time, an average single-to-noise ratio of 2.0 (defined in [47]), in 1.8 M monovalent-chloride salt, 100 mM Na–MOPS, pH 7.0, 0.1 mM EDTA solutions at 25°C, with an oxygen scavenging system of 2 mg/ml glucose, 1.8 mM Trolox, 100 units/ml glucose oxidase and 1000 units/ml catalase.
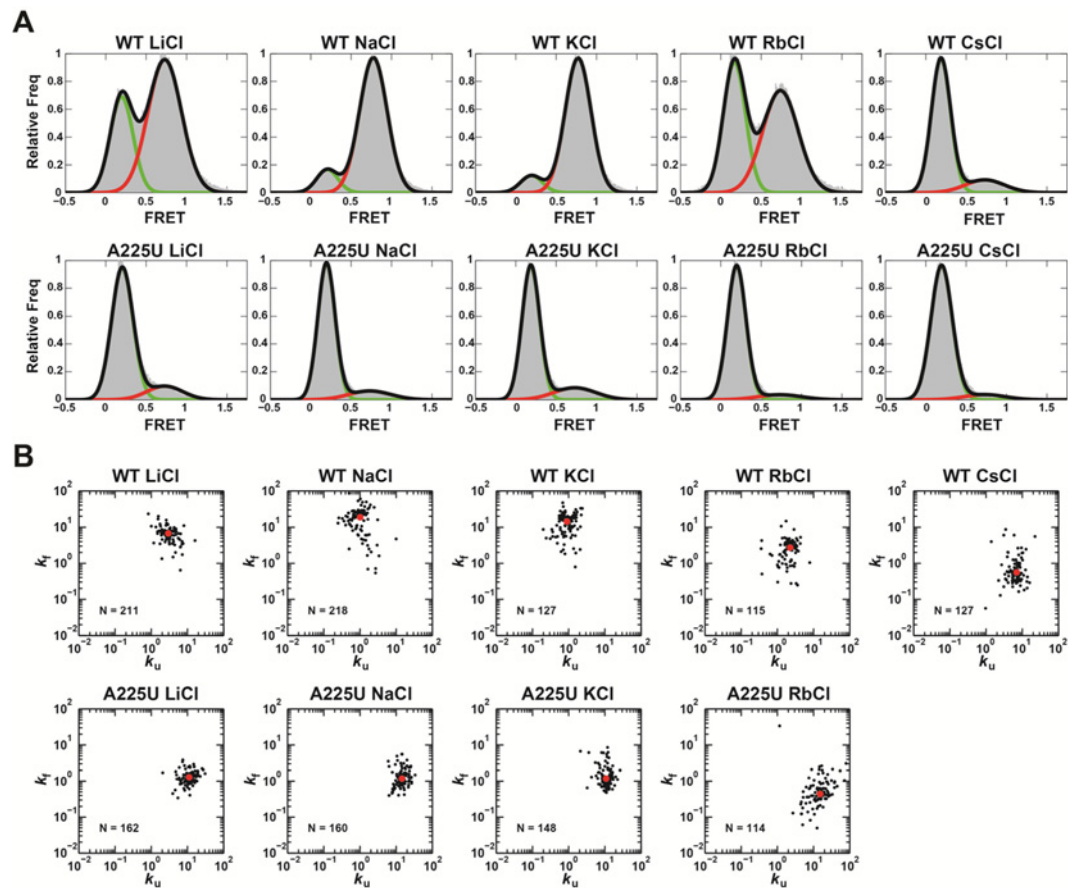

A-platform in the TLR makes multiple interactions with the monovalent cation based on the crystal structure of the *Azoarcus* group I intron [42] (Figure 1C) and thus the mutation A225U might be predicted to disrupt the association with the crystallographically-defined monovalent ion.

The observation that the preferential folding in Na^+ and K^+ over Li^+ is eliminated for A225U P4–P6 (Figure 3A, red) suggests that this folding preference arose from ion binding to this crystallographically-defined monovalent ion-binding site. Folding of the mutant is favoured in Li^+, Na^+ and K^+ relative to the larger Rb^+ or Cs^+ ions, consistent with expectations for a simple dependence on ion size. However, Li^+ did not give more favourable folding than Na^+ or K^+, as would have been predicted based solely on ion size and we do not know why such an effect is not seen. It is possible that the crystallographic site is not fully ablated or that a different weaker site, still with some specificity for Na^+ and K^+, remains. A225U mutant P4–P6 folds less well in each monovalent cation, with $\Delta\Delta G$ values ranging from ~3 kcal/mol (1 kcal ≡ 4184 J) in Na^+ or K^+ to ~1.5 kcal/mol

Figure 3 | **P4–P6 folding kinetics and thermodynamics compared with hydrated ion radius**

(**A**) Folding equilibria of wild-type (black) and mutant (red) P4–P6 compared with hydrated monovalent ion radius [11,51]. The folding equilibrium is defined as the ratio of the folding rate constant to unfolding rate constant, except for the data for A225U in CsCl, which is a limit obtained from the FRET distribution (Table 1) and is designated with an open circle and arrow. (**B** and **C**) Folding (**B**) and unfolding (**C**) rate constants of wild-type (WT) and mutant P4–P6 compared with ion size. The rate constants obtained for each molecule are plotted in small circles and the mean value of the population is plotted in large circles. (**D**) Effect on folding equilibrium of the A225U mutation compared with monovalent ion size, defined as $\Delta\Delta G = \Delta G_{A225U} - \Delta G_{WT}$. (**E**) Effect on the folding and (**F**) unfolding rate constants of the A225U mutation compared with ion size, defined as:

$$\Delta\Delta G^{\ddagger}_{fold} = -RT \ln\left(\frac{k_{fold,A225U}}{k_{fold,WT}}\right) \; ; \; \Delta\Delta G^{\ddagger}_{unfold} = -RT \ln\left(\frac{k_{unfold,WT}}{k_{unfold,A225U}}\right).$$
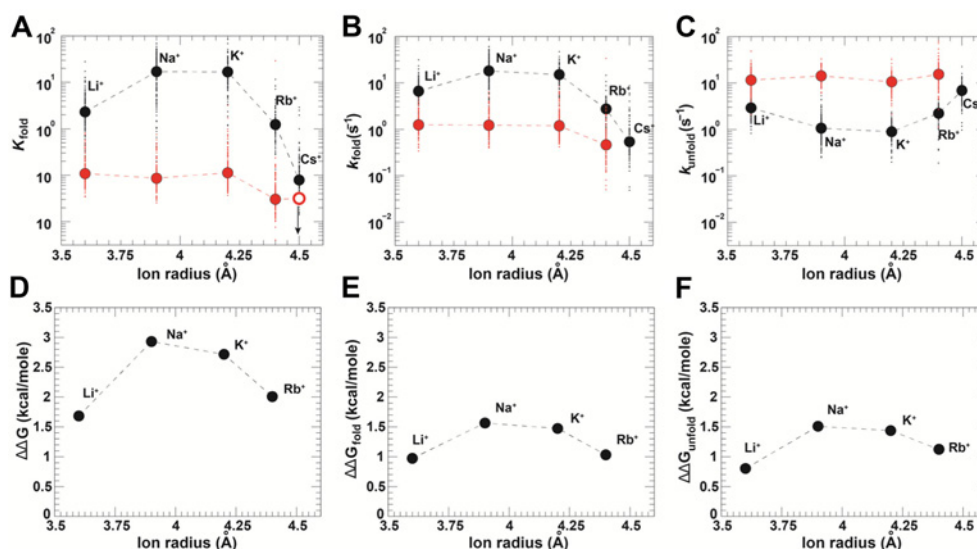
in Li$^+$ or Rb$^+$ (Figure 3D). These data indicate that there are deleterious effects of the mutation that remain in Li$^+$ or Rb$^+$, suggesting that the mutation disrupts interactions in addition to those involving monovalent ion binding.

The ion trends for wild-type and TLR-mutant P4–P6 closely match those observed for wild-type and a TLR mutant tecto-RNA [30]. As tecto-RNA also associates by TL–TLR interactions but has these interactions embedded within a different RNA context, these similarities suggest that the major contribution to the monovalent ion-specific effects lie within the TL–TLR and are not influenced by non-TL–TLR components of either tecto-RNA or P4–P6 RNA.

A simplified TL–TLR RNA, with these tertiary components tethered together via a flexible ssRNA linker, gave the same folding equilibrium and folding and unfolding rate constants in Na$^+$ and K$^+$ [43], consistent with the results in the more complex tecto- and P4–P6 constructs, but other monovalent cations were not investigated in the simplified TL–TLR system.

Rate effects of monovalent ions on P4–P6 folding

The folding and unfolding rate constants from the data in Figure 2(B) are compared, as a function of cation size, in Figure 3(B) and 3(C) respectively. For the mutant, there

is very little difference in these rate constants with folding in Rb$^+$ being ∼30% slower and unfolding possibly being slightly faster (red circles). These results stand in contrast with the dependence of the folding and unfolding rate constants for wild-type P4–P6 (black circles), with folding being ∼2-fold faster and unfolding ∼2–3-fold slower in Na$^+$ and K$^+$ relative to Li$^+$ and Rb$^+$ (Table 1). These results provide further support for the presence of a specific monovalent cation-binding site in wild-type P4–P6 and ablation of the site by the mutation.

The effects of the ions on the folding compared with unfolding rates can be considered in terms of phi analysis [44]. Phi analysis, borrowed from so-called linear free energy relationships in physical organic chemistry, compares equilibrium effects to effects on forward and reverse rate constants. Phi analysis has typically been applied to mutational effects, but here we consider the cation identity as our perturbant and other perturbations have also been analysed using similar frameworks [45].

The simplest scenarios for phi analysis are when the full effect of the perturbation on the equilibrium is manifested in either the folding or the unfolding rate constant. For example, if the full effect is on the folding rate constant, it is suggested that the interaction that is affected by the perturbation is not formed in the unfolded ground state but is (fully) formed sometime prior to the rate-limiting transition state. If the full

Table 1 | P4–P6 folding parameters obtained from smFRET

P4–P6 variants	Ion	Ion size* (Å)	$k_{fold}^†$ (s⁻¹)	$k_{unfold}^†$ (s⁻¹)	$K_{fold, kin}^†$	$K_{fold, FRETdist}^‡$	$\Delta G^§$ (kcal/mol)	SNR Cy3	SNR Cy5	Number of molecules	Trace lifetime (s)
WT	Li⁺	3.6	6.3±0.43	3.1±0.22	2.1±0.24	2.2	−0.42±0.50	2.3	2.1	211	11
	Na⁺	3.9	14.5±1.7	1.0±0.08	14.0±2.2	7.6	−1.5±0.67	2.8	2.2	218	17
	K⁺	4.2	12.2±1.5	0.90±0.08	13.5±1.8	9.4	−1.5±0.45	3.2	2.5	127	18
	Rb⁺	4.4	2.3±0.30	1.9±0.21	1.1±0.17	1.3	−0.07±0.48	2.3	2.4	115	22
	Cs⁺	4.5	0.59±0.09	6.3±0.54	0.093±0.018	0.20	1.4±0.53	2.6	2.8	127	32
A225U	Li⁺	3.6	1.3±0.10	11.3±0.82	0.11±0.011	0.17	1.3±0.34	2.2	2.2	162	14
	Na⁺	3.9	1.3±0.12	14.2±0.75	0.091±0.010	0.16	1.4±0.37	3.0	2.7	160	18
	K⁺	4.2	1.3±0.15	10.2±0.64	0.13±0.018	0.22	1.2±0.46	2.9	2.7	148	18
	Rb⁺	4.4	0.51±0.09	14.1±1.76	0.036±0.009	0.09	1.9±0.56	2.4	2.7	114	21
	Cs⁺	4.5	N.D.	N.D.	N.D.	<0.03‖	N.D.	N.D.	N.D.	153	27

*Ion size defined as the radius of the hydrated ions [51] and approximated as in [11] as the distance from the ion to the water oxygen atom in the first hydration shell plus 1.4 Å for the water layer.
†Error estimated through bootstrapping of measurements to determine 95% confidence intervals of the mean value.
‡$K_{fold, FRETdist}$ determined through a fit of the total FRET distribution of a population of molecules to two-Gaussians (Figure 2A) and taken as the ratio of the total time spent in the high FRET state relative to the low FRET state. These values are considered less accurate at high and low equilibrium values than the values obtained from the kinetic modelling, as the kinetic fits directly take into account the experimental noise.
§$\Delta G = - RT \ln(K_{fold, kin})$. Reported error is the standard deviation of the ΔG values for the population of molecules.
‖Value considered a limit as the small amount of apparent high FRET signal could arise from noise. N.D., not determined; SNR, average signal-to-noise ratio, defined in [47]. All reported data have a SNR > 1.5.

effect is on the unfolding rate constant, it is suggested that the interaction that is affected by the perturbation is formed in the folded state and broken in the unfolding process prior to the rate-limiting transition state; in the folding direction this would mean that the interaction is made after the rate-limiting transition state.

For the monovalent cation effects on P4–P6 folding, we have the more complex scenario in which the cation identity affects both folding and unfolding rate constants and to similar extents (Figures 3E and 3F), i.e., folding is faster in Na⁺ and K⁺ than Li⁺ by 2–3-fold and unfolding is slower by a similar extent. Although there are many possible interpretations for such complex behaviour, the simplest model would be that folding occurs with the monovalent cation associated prior to the rate-limiting transition state, helping to align or organize the TLR and rendering a higher fraction of TL–TLR encounters productive and subsequent to this transition state additional TL–TLR interactions are made that involve TLR components that are affected by the bound monovalent cation.

Implications

The ability of smFRET to measure rate and equilibrium constants over a wide range of stabilities and conditions allows comparisons to be made that would otherwise not be possible through bulk techniques. In this case we have determined the effects of a series of monovalent cations on folding of the P4–P6 RNA and a mutant of this RNA under identical ion concentration conditions. The measured equilibrium constants span a range of 400-fold and the rate constants, a range of 40-fold (Table 1).

An issue that often arises in smFRET studies is heterogeneity between different individual molecules, which can be an intrinsic property of the molecule or an artifact from damage or other covalent heterogeneity [39,46]. Our plots comparing the kinetic behaviour of all of the molecules allow ready visual inspection of heterogeneity and more rigorous tools to assess heterogeneity are available as needed [47]. The data of Figure 2(B) are reasonably tightly clustered and comparisons between wild-type and mutant P4–P6 and cation identity reveal clear differences (Table 1 and Figure 3).

Our results confirm and extend our knowledge of ion-specific behaviour of RNAs containing TL–TLR tertiary motifs. Whereas the larger Rb⁺ and Cs⁺ ions give less folding, as expected for their poorer screening ability [11,31], Na⁺ and K⁺ are both more effective in stimulating folding than the smaller Li⁺ ion, consistent with binding of these monovalent cations [18,34,42].

Finally, the observation of increased folding rates and decreased unfolding rates in Na⁺ and K⁺ and only with wild-type and not A225U mutant P4–P6, is consistent with a model in which Na⁺ or K⁺ binding to the TLR favours more structures within its structural ensemble that can productively bind to the TL. After the folding transition state, additional stabilizing interactions would be made according to this model that would decrease the rate of unfolding.

Detailed models such as this underscore the need to follow individual reaction steps during the folding process and to probe RNA conformational ensembles. Future work will allow the development of more generalizable and predictive models for RNA folding and will facilitate the dissection and manipulation of the complex behaviour of large and structured biological RNAs.

Funding

References

1 Cech, T.R. and Steitz, J.A. (2014) The noncoding RNA revolution-trashing old rules to forge new ones. Cell **157**, 77–94 CrossRef PubMed
2 Mercer, T.R. and Mattick, J.S. (2013) Structure and function of long noncoding RNAs in epigenetic regulation. Nat. Struct. Mol. Biol. **20**, 300–307 CrossRef PubMed
3 Rinn, J.L. and Chang, H.Y. (2012) Genome regulation by long noncoding RNAs. Annu. Rev. Biochem. **81**, 145–166 CrossRef PubMed
4 Warf, M.B. and Berglund, J.A. (2010) Role of RNA structure in regulating pre-mRNA splicing. Trends Biochem. Sci. **35**, 169–178 CrossRef PubMed
5 Garneau, N.L., Wilusz, J. and Wilusz, C.J. (2007) The highways and byways of mRNA decay. Nat. Rev. Mol. Cell Biol. **8**, 113–126 CrossRef PubMed
6 Montange, R.K. and Batey, R.T. (2008) Riboswitches: emerging themes in RNA structure and function. Annu. Rev. Biophys. **37**, 117–133 CrossRef PubMed
7 Kozak, M. (2005) Regulation of translation via mRNA structure in prokaryotes and eukaryotes. Gene **361**, 13–37 CrossRef PubMed
8 Akopian, D., Shen, K., Zhang, X. and Shan, S.O. (2013) Signal recognition particle: an essential protein-targeting machine. Annu. Rev. Biochem. **82**, 693–721 CrossRef PubMed
9 Hodak, J.H., Fiore, J.L., Nesbitt, D.J., Downey, C.D. and Pardi, A. (2005) Docking kinetics and equilibrium of a GAAA tetra loop-receptor motif probed by single-molecule FRET. Proc. Natl. Acad. Sci. U.S.A. **102**, 10505–10510 CrossRef PubMed
10 Chu, V.B., Lipfert, J., Bai, Y., Pande, V.S., Doniach, S. and Herschlag, D. (2009) Do conformational biases of simple helical junctions influence RNA folding stability and specificity? RNA **15**, 2195–2205 CrossRef PubMed
11 Bai, Y., Greenfeld, M., Travers, K.J., Chu, V.B., Lipfert, J., Doniach, S. and Herschlag, D. (2007) Quantitative and comprehensive decomposition of the ion atmosphere around nucleic acids. J. Am. Chem. Soc. **129**, 14981–14988 CrossRef PubMed
12 Draper, D.E. (2004) A guide to ions and RNA structure. RNA **10**, 335–343 CrossRef PubMed
13 Lipfert, J., Doniach, S., Das, R. and Herschlag, D. (2014) Understanding nucleic acid–ion interactions. Annu. Rev. Biochem. **83**, 813–841 CrossRef PubMed
14 Takamoto, K., Das, R., He, Q., Doniach, S., Brenowitz, M., Herschlag, D. and Chance, M.R. (2004) Principles of RNA compaction: insights from the equilibrium folding pathway of the P4-P6 RNA domain in monovalent cations. J. Mol. Biol. **343**, 1195–1206 CrossRef PubMed
15 Manning, G.S. (1978) The molecular theory of polyelectrolyte solutions with applications to the electrostatic properties of polynucleotides. Q. Rev. Biophys. **11**, 179–246 CrossRef PubMed
16 Fiore, J.L., Holmstrom, E.D., Fiegland, L.R., Hodak, J.H. and Nesbitt, D.J. (2012) The role of counterion valence and size in GAAA tetraloop–receptor docking/undocking kinetics. J. Mol. Biol. **423**, 198–216 CrossRef PubMed
17 Chu, V.B., Bai, Y., Lipfert, J., Herschlag, D. and Doniach, S. (2008) A repulsive field: advances in the electrostatics of the ion atmosphere. Curr. Opin. Chem. Biol. **12**, 619–625 CrossRef PubMed
18 Basu, S., Rambo, R.P., Strauss-Soukup, J., Cate, J.H., Ferré-D'Amaré, A.R., Strobel, S.A. and Doudna, J.A. (1998) A specific monovalent metal ion integral to the AA platform of the RNA tetraloop receptor. Nat. Struct. Biol. **5**, 986–992 CrossRef PubMed
19 Travers, K.J., Boyd, N. and Herschlag, D. (2007) Low specificity of metal ion binding in the metal ion core of a folded RNA. RNA **13**, 1205–1213 CrossRef PubMed
20 Szewczak, A.A., Kosek, A.B., Piccirilli, J.A. and Strobel, S.A. (2002) Identification of an active site ligand for a group I ribozyme catalytic metal ion. Biochemistry **41**, 2516–2525 CrossRef PubMed
21 Hougland, J.L., Kravchuk, A.V., Herschlag, D. and Piccirilli, J.A. (2005) Functional identification of catalytic metal ion binding sites within RNA. PLoS Biol. **3**, e277 CrossRef PubMed
22 Fica, S.M., Tuttle, N., Novak, T., Li, N.S., Lu, J., Koodathingal, P., Dai, Q., Staley, J.P. and Piccirilli, J.A. (2013) RNA catalyses nuclear pre-mRNA splicing. Nature **503**, 229–234 PubMed
23 Klein, D.J., Moore, P.B. and Steitz, T.A. (2004) The contribution of metal ions to the structural stability of the large ribosomal subunit. RNA **10**, 1366–1379 CrossRef PubMed
24 Shan, S.O., Yoshida, A., Sun, S.G., Piccirilli, J.A. and Herschlag, D. (1999) Three metal ions at the active site of the *Tetrahymena* group I ribozyme. Proc. Natl. Acad. Sci. U.S.A. **96**, 12299–12304 CrossRef PubMed
25 Frederiksen, J.K., Li, N.S., Das, R., Herschlag, D. and Piccirilli, J.A. (2012) Metal-ion rescue revisited: biochemical detection of site-bound metal ions important for RNA folding. RNA **18**, 1123–1141 CrossRef PubMed
26 Das, R., Travers, K.J., Bai, Y. and Herschlag, D. (2005) Determining the Mg^{2+} stoichiometry for folding an RNA metal ion core. J. Am. Chem. Soc. **127**, 8272–8273 CrossRef PubMed
27 Shan, S., Kravchuk, A.V., Piccirilli, J.A. and Herschlag, D. (2001) Defining the catalytic metal ion interactions in the *Tetrahymena* ribozyme reaction. Biochemistry **40**, 5161–5171 CrossRef PubMed
28 Harris, M.E. and Christian, E.L. (2009) Understanding the role of metal ions in RNA folding and function: lessons from RNase P, a ribonucleoprotein enzyme. In Springer Series in Biophysics (Martinac, B., ed.), pp. 183–213, Springer, Heidelberg CrossRef
29 Lipfert, J., Sim, A.Y., Herschlag, D. and Doniach, S. (2010) Dissecting electrostatic screening, specific ion binding, and ligand binding in an energetic model for glycine riboswitch folding. RNA **16**, 708–719 CrossRef PubMed
30 Lambert, D., Leipply, D., Shiman, R. and Draper, D.E. (2009) The influence of monovalent cation size on the stability of RNA tertiary structures. J. Mol. Biol. **390**, 791–804 CrossRef PubMed
31 Bai, Y., Chu, V.B., Lipfert, J., Pande, V.S., Herschlag, D. and Doniach, S. (2008) Critical assessment of nucleic acid electrostatics via experimental and computational investigation of an unfolded state ensemble. J. Am. Chem. Soc. **130**, 12334–12341 CrossRef PubMed
32 Jaeger, L., Westhof, E. and Leontis, N.B. (2001) TectoRNA: modular assembly units for the construction of RNA nano-objects. Nucleic Acids Res. **29**, 455–463 CrossRef PubMed
33 Wu, L., Chai, D., Fraser, M.E. and Zimmerly, S. (2012) Structural variation and uniformity among tetraloop-receptor interactions and other loop-helix interactions in RNA crystal structures. PLoS ONE **7**, e49225 CrossRef PubMed
34 Uchida, T., He, Q., Ralston, C.Y., Brenowitz, M. and Chance, M.R. (2002) Linkage of monovalent and divalent ion binding in the folding of the P4-P6 domain of the *Tetrahymena* ribozyme. Biochemistry **41**, 5799–5806 CrossRef PubMed
35 Cate, J.H., Gooding, A.R., Podell, E., Zhou, K., Golden, B.L., Kundrot, C.E., Cech, T.R. and Doudna, J.A. (1996) Crystal structure of a group I ribozyme domain: principles of RNA packing. Science **273**, 1678–1685 CrossRef PubMed
36 Cate, J.H., Hanna, R.L. and Doudna, J.A. (1997) A magnesium ion core at the heart of a ribozyme domain. Nat. Struct. Biol. **4**, 553–558 CrossRef PubMed
37 Murphy, F.L. and Cech, T.R. (1993) An independently folding domain of RNA tertiary structure within the *Tetrahymena* ribozyme. Biochemistry **32**, 5291–5300 CrossRef PubMed
38 Szewczak, A.A. and Cech, T.R. (1997) An RNA internal loop acts as a hinge to facilitate ribozyme folding and catalysis. RNA **3**, 838–849 PubMed
39 Greenfeld, M., Solomatin, S.V. and Herschlag, D. (2011) Removal of covalent heterogeneity reveals simple folding behavior for P4-P6 RNA. J. Biol. Chem. **286**, 19872–19879 CrossRef PubMed
40 Joo, C., Balci, H., Ishitsuka, Y., Buranachai, C. and Ha, T. (2008) Advances in single-molecule fluorescence methods for molecular biology. Annu. Rev. Biochem. **77**, 51–76 CrossRef PubMed
41 Cate, J.H., Gooding, A.R., Podell, E., Zhou, K., Golden, B.L., Szewczak, A.A., Kundrot, C.E., Cech, T.R. and Doudna, J.A. (1996) RNA tertiary structure mediation by adenosine platforms. Science **273**, 1696–1699 CrossRef PubMed

42 Adams, P.L., Stahley, M.R., Gill, M.L., Kosek, A.B., Wang, J.M. and Strobel, S.A. (2004) Crystal structure of a group I intron splicing intermediate. RNA **10**, 1867–1887 CrossRef PubMed

43 Holmstrom, E.D., Fiore, J.L. and Nesbitt, D.J. (2012) Thermodynamic origins of monovalent facilitated RNA folding. Biochemistry **51**, 3732–3743 CrossRef PubMed

44 Fersht, A.R., Matouschek, A. and Serrano, L. (1992) The folding of an enzyme. 1. Theory of protein engineering analysis of stability and pathway of protein folding. J. Mol. Biol. **224**, 771–782 CrossRef PubMed

45 Sosnick, T.R., Krantz, B.A., Dothager, R.S. and Baxa, M. (2006) Characterizing the protein folding transition state using psi analysis. Chem. Rev. **106**, 1862–1876 CrossRef PubMed

46 Solomatin, S.V., Greenfeld, M., Chu, S. and Herschlag, D. (2010) Multiple native states reveal persistent ruggedness of an RNA folding landscape. Nature **463**, 681–684 CrossRef PubMed

47 Greenfeld, M., Pavlichin, D.S., Mabuchi, H. and Herschlag, D. (2012) Single Molecule Analysis Research Tool (SMART): an integrated approach for analyzing single molecule data. PLoS ONE **7**, e30024 CrossRef PubMed

48 Solomatin, S. and Herschlag, D. (2009) Methods of site-specific labeling of RNA with fluorescent dyes. Methods Enzymol. **469**, 47–68 CrossRef PubMed

49 Greenfeld, M. and Herschlag, D. (2010) Measuring the energetic coupling of tertiary contacts in RNA folding using single molecule fluorescence resonance energy transfer. Methods Enzymol. **472**, 205–220 CrossRef PubMed

50 Shi, X., Bisaria, N., Benz-Moy, T.L., Bonilla, S., Pavlichin, D.S. and Herschlag, D. (2014) Roles of long-range tertiary interactions in limiting dynamics of the *Tetrahymena* group I ribozyme. J. Am. Chem. Soc. **136**, 6643–6648 CrossRef PubMed

51 Ohtaki, H. and Radnai, T. (1993) Structure and dynamics of hydrated ions. Chem. Rev. **93**, 1157–1204 CrossRef